Electrochimica Acta 169 (2015) 37–45

Contents lists available at ScienceDirect

Electrochimica Acta

journal homepage: www.elsevier.com/locate/electacta

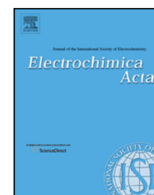

Thermoelectric properties of electrodeposited tellurium films and the sodium lignosulfonate effect

Begoña Abad [a], Marta Rull-Bravo [a], Stephen L. Hodson [b], Xianfan Xu [b], Marisol Martin-Gonzalez [a,*]

[a] IMM-Instituto de Microelectrónica de Madrid (CNM-CSIC), Isaac Newton 8, PTM, E-28760 Tres Cantos, Madrid, Spain
[b] School of Mechanical Engineering, Birck Nanotechnology Center, Purdue University, West Lafayette, Indiana 47907 USA

ARTICLE INFO

Article history:
Received 28 November 2014
Received in revised form 13 March 2015
Accepted 10 April 2015
Available online 13 April 2015

Keywords:
Electrochemical deposition
surfactant
grain size
electrical conductivity
Seebeck coefficient
thermal conductivity

ABSTRACT

The effect of the addition of a surfactant, sodium lignosulfonate (SLS), on the thermoelectric properties of tellurium films prepared by electrochemical deposition is studied. The growth mechanism is found to have an important role in the thermoelectric properties since the grain size of the films is sharply reduced when the surfactant is added to the solution. For this reason, the electrical resistivity of the tellurium films when the surfactant is not added is 229 $\mu\Omega$·m, which is lower than 798 $\mu\Omega$·m with SLS. The Seebeck coefficient values are not influenced, with values in the vicinity of 285 μV/K for both solutions. The power factor resulted higher values than previous works, reaching values of 280 $\mu W/m{\cdot}K^2$ (without SLS) and 82 $\mu W/m{\cdot}K^2$ (with SLS) at room temperature. Finally, the thermal conductivity was measured by means of the Photoacoustic technique, which showed values of the order of 1 W/m·K for both solutions, which is a factor of 3 less than the bulk value of tellurium. A notable observation is that the power factor and the thermal conductivity of electrodeposited tellurium films have the same order of magnitude of bismuth telluride films grown by electrodeposition. The figure of merit is estimated to be approximately one order of magnitude higher than the bulk value, 0.09 without SLS and 0.03 with SLS, both at room temperature.

© 2015 Elsevier Ltd. All rights reserved.

1. INTRODUCTION

Tellurium is a p-type semiconductor with a narrow band-gap (0.34 eV) and a highly anisotropic crystal structure. It consists of helical chains, which are bound by covalent unions between the atoms and bound with other chains by van der Waals interactions. These chains turn into a hexagonal lattice whose c axis is perpendicular to the hexagonal base or parallel to the helical chains [1], see Fig. 1. In recent years, tellurium thin films have been studied for applications such as gas sensors (detection of nitrogen dioxide or ammonia) [2], piezoelectrics [3], photoconductors [4], photonic crystals [5], submillimeter wave detectors [6], and thermoelectric devices [7]. Thermoelectricity is the ability of the materials to convert heat into electricity and the inverse effect. The efficiency of thermoelectric materials is related to their figure of merit, which is given by $zT = S^2\sigma/k$, where S is the Seebeck coefficient, σ is the electrical conductivity and κ is the thermal conductivity [8]. In order to obtain a maximum figure of merit, the optimization of the thermoelectric parameters is needed. For this purpose, diverse choices of materials, preparation routes, and dopants are being studied. As a thermoelectric material, bulk tellurium presents a high Seebeck coefficient of approximately 500 μV/K along the c-axis direction [7], where the positive sign indicates a p-type conduction. The electrical resistivity was found to be between around 2900 and 5000 $\mu\Omega$·m in the direction parallel and perpendicular to the c-axis respectively at room temperature [9],[10]. The thermal conductivity is approximately 3 W/m·K for the bulk material that depends on the crystal orientation, being 3.37 W/m·K and 1.96 W/m·K for the direction parallel and perpendicular direction to the c-axis at room temperature [11],[12]. Assuming the same value of the Seebeck coefficient in both directions and taking the aforementioned electrical resistivity and thermal conductivity values for each direction, a zT of 0.008 for both the direction parallel and perpendicular to de c-axis at room temperature can be calculated. Due to the p-type character of tellurium, it is interesting the study of its thermoelectric properties since it could serve as the p-type counterpart of a thermoelectric device.

The electronic transport properties, which depend on the structure, growth and crystal orientation of tellurium samples, are

* Corresponding author.
E-mail address: marisol@imm.cnm.csic.es (M. Martin-Gonzalez).

http://dx.doi.org/10.1016/j.electacta.2015.04.063
0013-4686/© 2015 Elsevier Ltd. All rights reserved.

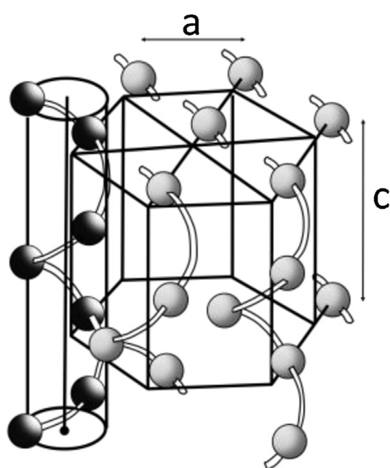

Fig. 1. Crystal structure of tellurium.

being studied with various preparation techniques and within different temperature ranges [9],[13–17]. Goswami et al. studied the semiconducting properties of films grown by vacuum deposition and observed that the Seebeck coefficient exhibited no temperature dependence near room temperature [18]. The Seebeck coefficient of tellurium prepared by vacuum deposition was intensively studied by Phahle [17] and later by Damodara et al. [19], which showed a value as high as 500 μV/K and 400 μV/K, respectively, at room temperature; in agreement with the previously obtained value [18]. Recently, Bodiul et al. [7] studied the thermoelectric properties of both films and monocrystalline whiskers of tellurium fabricated by a vacuum-condensation method. The power factor of these thin films, defined as $S^2\sigma$, reached 100 $\mu W/m{\cdot}K^2$ with a Seebeck coefficient of approximately 350 μV/K and a value of the electrical conductivity of 1100 μΩ·m. However, few studies on tellurium by electrodeposition were previously conducted. Jiang et al. [20] reported measurements of the Seebeck coefficient of tellurium films grown by electrochemical deposition on polyaniline-coated macroporous phenolic foam which corresponded to a maximum thermopower value of 342 μV/K at 473K [20].

Electrochemical deposition is based on the reduction of ions from aqueous, organic, ionic or molten salt electrolytes. In order to produce the reaction (reduction) of the charged particles at the interface between solid electrode and liquid solution, it is necessary to have an external power supply which provides the electrons. This technique provides an attractive alternative route to the fabrication of high-quality nanostructured compounds [21–25], thus offering several comparative advantages to other methods used to prepare tellurium structures such as solvothermal [26] and hydrothermal techniques [27], microwave-assisted method [28], and vacuum deposition [13]. These advantages include room temperature fabrication, no vacuum, high deposition rates and structure control by different parameters like potential, solution or the use of surfactants [29]. Moreover, electrochemical deposition is a low cost technique that is easily transferrable to the industry.

Another important point to highlight is that the electroreduction of tellurium is on the basis of the electrodeposition mechanism of several telluride-based chalcogenides such as CdTe for solar cells [30], ZnTe for optoelectronics and non-linear optics [31], or PbTe [32,33] and Bi_2Te_3 [34–36] for thermoelectric materials. The mechanism of electrodeposition of those semiconductors and their ternary alloys occurs by an induced codeposition mechanism after the electrochemical reduction of tellurium from solution. The tellurium is initially nucleated by reduction at the cathode with any of the following reactions [34]:

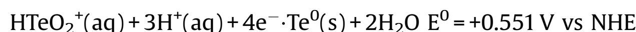
$$HTeO_2^+(aq) + 3H^+(aq) + 4e^- \cdot Te^0(s) + 2H_2O \quad E^0 = +0.551\ V\ vs\ NHE$$

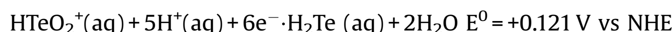
$$HTeO_2^+(aq) + 5H^+(aq) + 6e^- \cdot H_2Te\ (aq) + 2H_2O \quad E^0 = +0.121\ V\ vs\ NHE$$

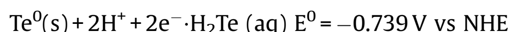
$$Te^0(s) + 2H^+ + 2e^- \cdot H_2Te\ (aq) \quad E^0 = -0.739\ V\ vs\ NHE$$

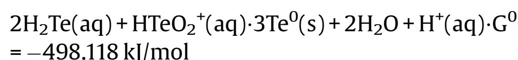
$$2H_2Te(aq) + HTeO_2^+(aq) \cdot 3Te^0(s) + 2H_2O + H^+(aq) \cdot G^0 = -498.118\ kJ/mol$$

and reacts with cadmium [37], zinc [37], lead [38] or bismuth [34] to produce the compound. For the aforementioned reasons, modification of the quality of the electrodeposited tellurium could be interesting in order to understand the performance of these compounds. A possible method to change the growth mechanism and control the quality of the films is to add surface active agents, i.e., surfactants. Sodium lignosulfonate (SLS) is a surfactant that was found to modify the quality of the films grown by electrodeposition [29]. However, the inherent effect of SLS on tellurium growth has yet to be studied. The main objective of this work is to understand the effect of sodium lignosulfonate on the electrodeposition and the thermoelectric behavior of tellurium by studying the influence of surfactant addition to the structural, morphological and thermoelectric properties.

2. EXPERIMENTAL SECTION

Tellurium thick films have been prepared by electrochemical deposition in an aqueous solution consisting of 1.10^{-2} M $HTeO_2^+$, 1 M HNO_3 with and without 0.06 g/L sodium lignosulfonate (SLS). The chemical compounds used in the solution were Fluka Chemika® tellurium powder, lignosulfonic acid sodium salt from Sigma Aldrich® and Panreac® 65% nitric acid. The preparation of the solution consists of dissolving the $HTeO^{2+}$ in nitric acid and then adding deionized water to reach the desired volume. The employed electrochemical cell is based on a conventional three electrode cell configuration. The working electrode consists of a 150 nm platinum layer evaporated via electron-beam evaporation onto a silicon wafer (1 0 0) with the aid of a 5 nm chromium layer between the silicon and the platinum to improve the adhesion. The reference electrode is Ag/AgCl 3 M electrode and a platinum mesh acts as a counter electrode. Cyclic voltammograms (CVs) and chronoamperometries were performed in a bi-potentiostat (Eco Chemie, Model AUT302.0) governed by the software Nova 1.8. All the experiments were conducted at room temperature. The potential limits of the CVs were chosen to be between −0.5 V and 1.0 V *vs.* the reference electrode and the scanning rate was set at 0.01 V/s. The films were grown by applying the potential for one hour, which yield samples whose thicknesses are in the range of several microns that completely cover the surface of the electrode.

The morphology of the films has been studied by a Philips® XL305-FEG field emission scanning electron microscope (FE-SEM) with an accelerating voltage of 10 kV. The structural characterization was examined by X-ray diffraction (XRD) in a Philips® X'Pert four circle diffractometer with CuKα X-ray radiation.

Prior to the thermoelectric measurements, the films were lifted-off to avoid the influence of the platinum on the properties of interest. For this purpose, an epoxy adhesive (Araldit® high temperature from Ceys®) was used to glue the film to a glass slide and was allowed to dry overnight. The samples were then immersed in liquid nitrogen in such a way that the difference in

thermal expansion coefficients allowed for the detachment of the tellurium film adhered to the glass substrate from the platinum on silicon wafer.

The Seebeck coefficient, S, and electrical resistivity ($\rho = 1/\sigma$) were simultaneously measured with a LSR-3 Linseis equipment. Before the measurements, the thickness of the films was measured by means of a Veeco® Dektak stylus profilometer system for the calculation of the electrical resistivity from the resistance measurement. The electrical resistivity was measured by a four-point probe method and the Seebeck coefficient was obtained by setting two different temperature gradients of approximately 1 °C and 8 °C between the ends of the films. The slope between the temperature differences and the generated Seebeck voltage allows the Seebeck coefficient to be obtained. Both magnitudes, electrical conductivity and Seebeck coefficient, were measured in a range of temperature from approximately 30 °C to 105 °C in order to not exceed the maximum temperature that epoxy can endure. To ensure the accuracy of the experiment, multiple steady state measurements at each temperature point were performed.

An experimental system based on the Photoacoustic technique was employed to measure the thermal conductivity of the films in the cross-plane direction. This technique is based on the Photoacoustic effect in which incident modulated radiation periodically heats the sample and subsequently causes the air in contact with the surface to expand and contract similar to a thermal piston. This effect causes acoustic waves which are detected by a microphone. By comparing the incident signal with the recorded signal, the thermal properties of the sample can be obtained by using a multilayer model developed by Hu et al. [39]. The apparatus consists of a lab-design experimental setup, Fig. 2, where a PMMA Photoacoustic cell was modeled in such a way acoustic resonances are avoided. The samples were radiated by a fiber-couple laser diode LDF-10 series Alphalas GmbH of 980 nm with an optical power of 260 mW. The signal was detected by a G.R.A.S. 46 BL 1/4" CCP Pressure Microphone Set. That signal is then filtered and amplified by a power module type 12AQ G.R.A.S. Finally, a Signal Recovery Model 7270 DSP Lock-in Amplifier was used to obtain the required signal. Prior to the measurements, the thicknesses of the films were measured under the same conditions where the measurement occurred such that experimental errors were minimized. Moreover, an 80 nm titanium layer was evaporated via electron-beam evaporation onto the samples in order to absorb the laser beam. Some of the samples presented in this work were measured at Purdue University to establish the accuracy of the measurements.

Regarding the experimental errors, the crystallite size, power factor and figure of merit error was calculated by using the law of propagation of error. For the crystallite size an error of 10% was assumed for the FWHM and the power factor error was calculated by taking 10% for the electrical resistivity and 5% for the Seebeck coefficient. In the case of the thermal conductivity, the Photoacoustic technique presents an associated error around 10% for these films which arise from the properties of the samples, the thickness and the random error obtained by measuring several times each sample.

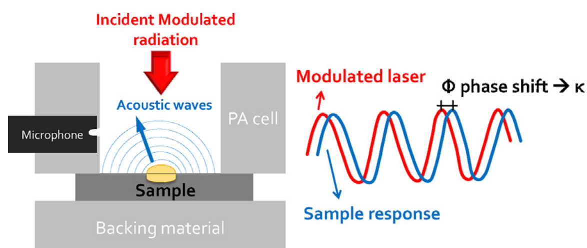

Fig. 2. Photoacoustic technique setup.

3. RESULTS AND DISCUSSION

Cyclic voltammograms (CV) were made in order to study the different deposition mechanism and to find the optimal deposition potential. A CV on a platinum working electrode was carried out using a Ag/AgCl reference electrode for each solution. Fig. 3 shows the main tellurium reduction peaks without and with SLS at −0.13 V and −0.20 V, respectively. The main cathodic peak can be identified with the reduction of the $HTeO_2^+$ to Te, found also by Martín-González *et al.* [34], who studied the electrochemical behavior of tellurium without additives. This shift can be explained by the competing adsorption of the surfactant onto the electrode, which hindered the reduction of tellurium by decreasing the number of reduction sites available at the electrode surface. The current plateau when the surfactant is added to the solution presents lower current density than in the absence of the surfactant. This indicates that surfactant molecules could be adsorbed onto the platinum surface, thus decreasing the current density, j_p.

When the potential is more negative than −0.3 V, another pronounced cathodic wave is found in both solutions corresponding to the hydrogen evolution. On the other hand, only one oxidation peak is present in the oxidation region with a potential of approximately $V = 0.6$ V in both cases. It is noteworthy that there is a remarkable difference between the oxidation area peaks. Since the working electrode area was the same for both CVs, this difference could be related to the total charge passing through the electrode and the total amount of tellurium deposited on the electrode surface. As it can be seen in Fig. 3, the area of the oxidation peak in the CV carried out from the solution with SLS is smaller than the one performed without SLS. That difference indicates that the total charge going through the electrode is lower in the case of the CV with SLS so that the amount of tellurium deposited on the electrode is smaller. That could be confirmed by calculating the charges of the anodic peak (Q_+) and cathodic region calculated without hydrogen evolution (Q_-) part from both CV. In the case of the solution without SLS $Q_- = -56.1$ mC and $Q_+ = 40.7$ mC, whereas in the case of the solution with SLS,

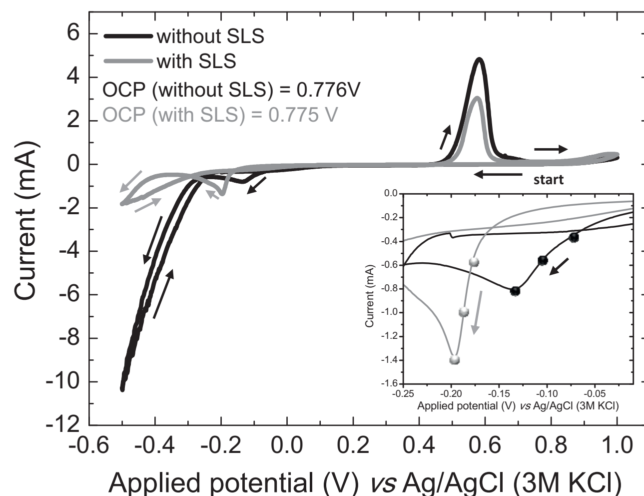

Fig. 3. Cyclic Voltammogram of $HTeO_2^+$ 0.01 M in 1 M HNO_3 with (gray) and without (black) 0.06 g/L SLS with a scan rate of 0.01 V/s at room temperature. The inset shows the main reduction peak for each solution and the three different points were the electrochemical depositions were performed. Arrows indicate the scan direction of the CV.

Q_{-} = −44.3 mC and Q_{+} = 21.1 mC. This indicates the inhibitor character of the surfactant on tellurium electrodeposition.

The electrochemical depositions were carried out at three different potentials along the reduction peak (−0.13 V, −0.10 V and −0.07 V in the case of the solution without SLS and −0.18 V, −0.19 V and −0.20 V for the solution with SLS, see inset on Fig. 3).

Fig. 4 shows the X-Ray diffractograms of the films grown at different applied potentials along with the reference pattern of tellurium powder (JCPDS 36-1452) for both solutions with and without SLS. The XRD was measured after detaching the films from the substrate in such a way that neither platinum nor silicon peaks were present.

Different diffraction peaks can be observed and are indexed to the hexagonal phase of tellurium reference pattern as shown in Fig. 4. For the solution without SLS, the (1 0 1) diffraction peak located at 2θ = 27.563° is the sharpest for the three films as in the reference polycrystalline pattern. The second order diffraction peak, (2 0 2) placed at 2θ = 56.878° is also found in the diffractogram. Less intense diffraction maxima like (1 0 2) at 2θ = 38.261° and (1 1 0) at 2θ = 40.446° can be observed. As it can be seen in the standard pattern, the diffraction peaks for (1 0 1), (1 0 2) and (1 1 0) are the strongest so that the films grown without SLS present a microstructure similar to a polycrystalline pattern. However, the relative intensity between these peaks changes as a function of the applied potential. Moreover, other even less intense peaks are present, such as (1 0 0), (1 1 1), (2 0 1) and (1 1 3). The full width at half maximum (FWHM) of the (1 0 1) diffraction peak has been measured given different values as a function of the applied potential. The obtained values are 0.15°, 0.16° and 0.21° for the −0.13 V, −0.10 V, and −0.07 V, respectively. The smaller the FWHM, the bigger the crystallite size is, and hence, a more negative applied voltage produced larger grain sizes.

In the X-Ray diffractogram of the films grown from the solution with SLS, the (1 0 1) diffraction peak is the strongest of the three films and the weaker (2 0 2) diffraction peak is also found. Moreover, as in the previous case, a textured direction cannot be distinguished since other diffraction peaks can be observed in these films, such as (1 0 0), (1 0 2), (1 1 0), (1 1 1) and even (0 0 3). The FWHM of the (1 0 1) diffraction peak has also been measured giving different values as a function of the applied potential. The obtained values are 0.33°, 0.36° and 0.32° for the −0.20 V, −0.19 V and −0.18 V, respectively. The FWHM values are quite similar for the three films, probably due to the slight change in the applied potential.

Both types of solutions presented sharp peaks, indicating that the films are crystalline. Moreover, as these films are not highly oriented in a specific crystal orientation, a polycrystalline character can be assumed in all the cases. However, the relative intensity between the highest diffraction peak (1 0 1) and (1 1 0) has considerably changed when adding the surfactant. Basically, the direction (1 1 0) seems to be slightly inhibited by the presence of the surfactant. Moreover, regarding the FWHM, it is noteworthy that the crystallite size of the films grown without SLS is larger than in the case when SLS is used.

Figs. 5 and 6 show the morphology of the tellurium films grown at the three different potentials for both solutions. Regarding the films grown from the solution without SLS, the most negative deposition potential yields the largest particle size. However, from the cross-section views it can be seen that the microstructure order decreases when the applied potential is made more negative. These images also show a bundle of structures with cavities growing directly from the substrate. This kind of growth is possibly due to the highly anisotropic crystal growth of the trigonal tellurium [40,41]. The crystals are randomly oriented initially from a nucleation site in such a way that the XRD pattern shows the polycrystalline character of the films. The thicknesses of the films were measured with the profilometer providing values, 4.6 μm, 3.4 μm, 3.0 μm for V = −0.13 V, V = −0.10 V and V = −0.07 V, respectively, in good agreement with the those estimated from the SEM images, 4.5 μm, 3.5 μm and 3.0 μm for V = −0.13 V, V = −0.10 V and V = −0.07 V, respectively.

In the case of the solution with SLS, minimal differences can be appreciated between the different applied potentials where the cross-sections show that the films have grown in a columnar way. Moreover, the top views of the films show arrow-like morphology in such a way that a large quantity of crystals can be observed. In this case, the type of growth is completely different than without SLS. The typical tellurium growth mechanism is interrupted by means of the surfactant which acts as an anti-coagulation agent, limiting the growth in the typical directions. SLS inhibits tellurium particle growth, modifying the crystal growth behavior such that smoother and more compact films are obtained as revealed in the SEM images. The thicknesses of the films measured with the profilometer, 2.9 μm, 2.9 μm, 2.5 μm for V = −0.20 V, V = −0.19 V and V = −0.18 V, are in good accordance with those calculated from the SEM images, 3.0 μm, 3.5 μm, 3.0 μm for V = −0.20 V, V= −0.19 V and V = −0.18 V respectively, (see Fig. 6).

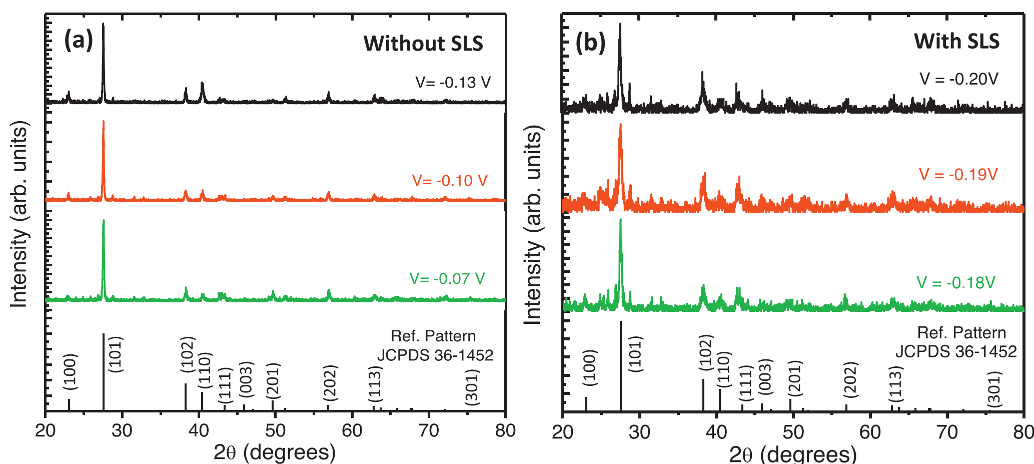

Fig. 4. X-ray diffractograms for the films grown in three different applied potentials from both solutions (a) without and (b) with SLS.

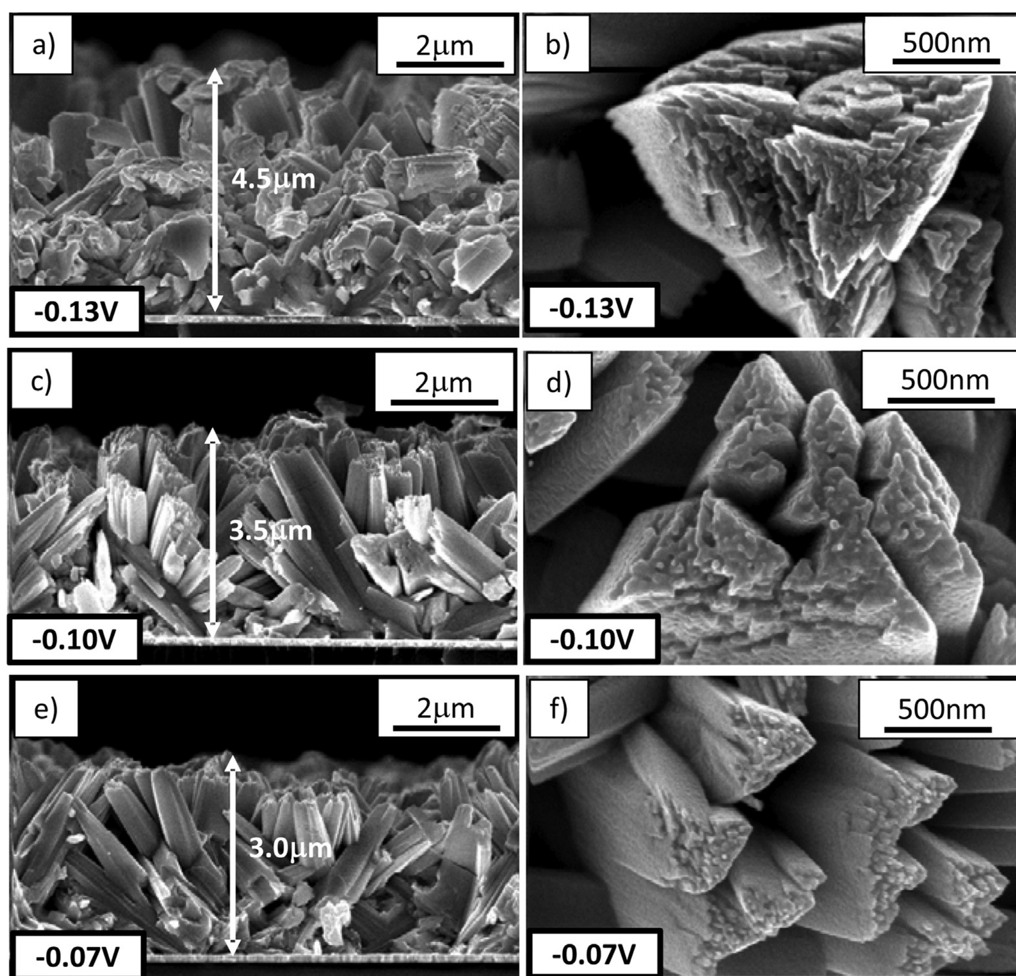

Fig. 5. FE-SEM images of the as-grown electrodeposited films without SLS. (a) Cross section and (b) in-plane image of the film grown at −0.13 V, (c) cross-section and (d) and in-plane image of the film grown at −0.10 V and (e) cross-section and (f) in-plane image of the film grown at −0.07 V. The thicknesses of the films are marked with an arrow.

The in-plane electrical resistivity and the Seebeck coefficient have been measured as a function of temperature for the films prepared with and without SLS. Then, the power factor was calculated in order to find the conditions that will provide the highest efficiency. Finally, the thermal conductivity was also measured in the out of plane direction of the films.

As seen in Fig. 7, the electrical resistivity decreases with temperature which is the typical behavior of a semiconductor. The minimum values are obtained at 105 °C, reaching a value of 197 $\mu\Omega\cdot$m for the film prepared without SLS at −0.07 V and a value of 509 $\mu\Omega\cdot$m for the film grown at −0.20 V with SLS. It should be noted that the near-to-room temperature values (35 °C) 229 $\mu\Omega\cdot$m (without SLS) and 798 $\mu\Omega\cdot$m (with SLS), are obtained for both solutions, respectively. This value is an order of magnitude lower than the values obtained by Bottom et al. for a single crystal, where 5600 $\mu\Omega\cdot$m and 2900 $\mu\Omega\cdot$m were obtained for the perpendicular and parallel direction to the principal axis, i.e, c axis, respectively [10]. This sharp reduction in the electrical resistivity could be related to structural defects in the samples. In the case of tellurium films, one can find adsorbed surface impurities, surface states or a potential barrier at the grain boundaries, among other structural defects. The most common mechanism previously reported is the surface states which appear on the surface of tellurium films and can act as electrically active defects [16]. From the slope between the logarithm of the electrical resistivity, ρ, against 1/T, where T is the temperature, the activation energy of these impurities in the band gap can be obtained since the electrical resistivity measurements are in the vicinity of the temperature where the electrical activation of those impurities takes place [17]. The activation energies along with the electrical resistivity at room temperature of the films are shown in Fig. 8, where the values range from 50 meV to 68 meV in the case of the films grown without SLS and from 87 meV to 108 meV with SLS. These values are in agreement with previously works. Phahle et al. calculated an activation energy of 180meV and an electrical resistivity around 500 $\mu\Omega\cdot$m at a similar temperature range and Goswami et al. obtained activation energy values from 178 meV to 58 meV, for thermal evaporation grown samples [17,18]. A similar trend between the activation energy and the electrical resistivity can be appreciated for the films with and without SLS, which indicates that the electrical resistivity is closely linked to the impurity level. It is observed that the impurities associated with the use of SLS present deeper levels, and hence, higher activation energy than in the case of the films grown without SLS. For this reason, the electrical resistivity is lower when the SLS is not used.

For films grown without SLS, the electrical resistivity increases when increasing the driving force during electrodeposition, which contradicts the notion that the sample deposited at −0.13 V has bigger grain sizes. However, by observing the SEM images in Fig. 5, poor ordering of the crystals is apparent when compared to −0.10 and −0.07 V films.

Regarding the films grown with SLS, since the surfactant inhibits the natural growth of tellurium, the crystallite size is considerably smaller than that of films grown without SLS. As a

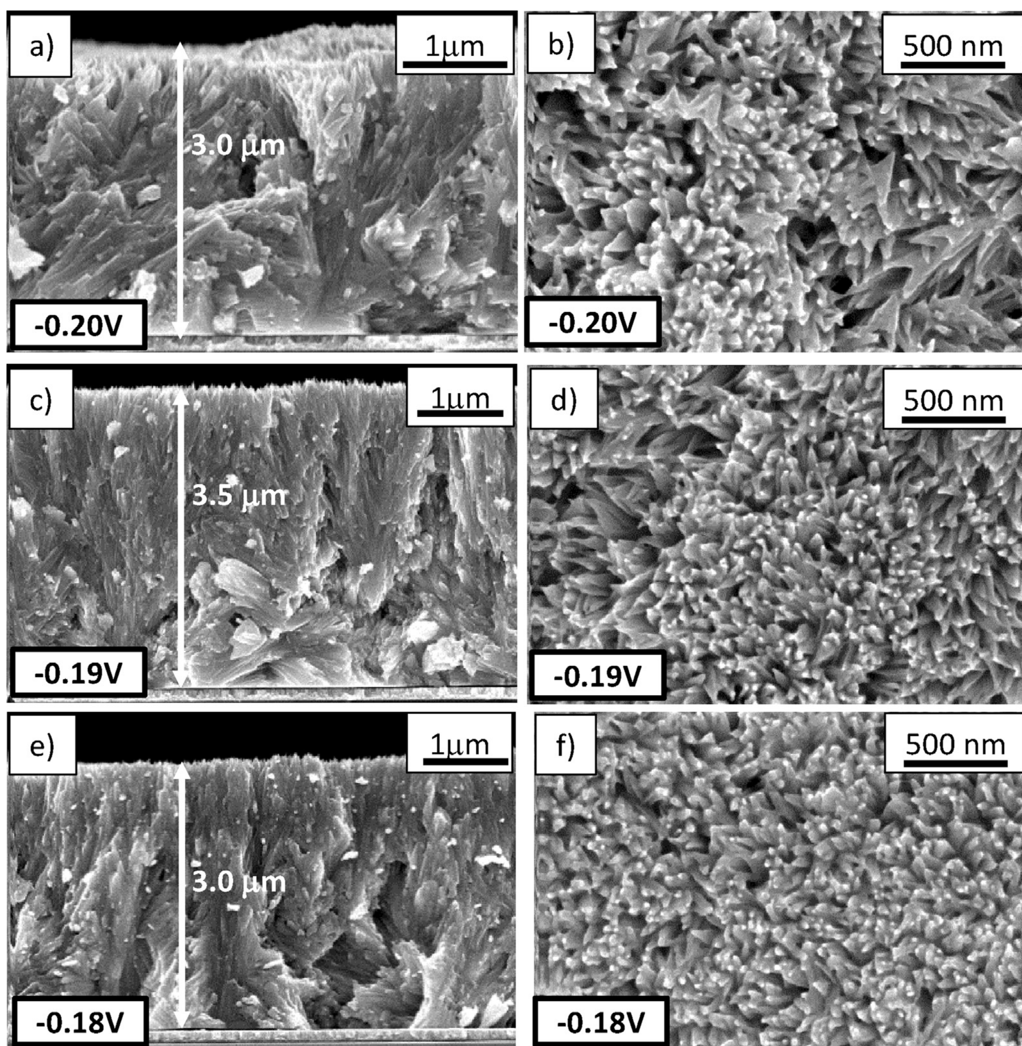

Fig. 6. FE-SEM images of the as-grown electrodeposited films with SLS. (a) Cross section and (b) in-plane image of the film grown at −0.20 V, (c) cross-section and (d) in-plane image of the film grown at −0.19 V and (e) cross-section and (f) in-plane image of the film grown at −0.18 V. The thicknesses of the films are marked with an arrow.

result, these films present more grain boundaries which explain the increase in the electrical resistivity. This result is in agreement with previous works where an increase in the electrical resistivity was observed in Bi_2Te_3 films when using SLS [29]. In the case of the films grown with SLS, when the driving force of the solution is larger the electrical resistivity is lower.

Regarding the Seebeck coefficient, Fig. 9 indicates that all the films exhibit p-type conduction. Moreover, the thermoelectric

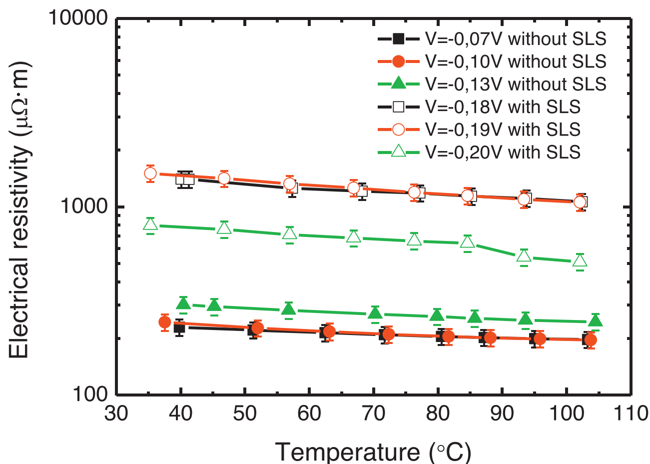

Fig. 7. Electrical resistivity of the films grown at different applied potentials for both solutions, with (open symbols) and without (solid symbols) SLS.

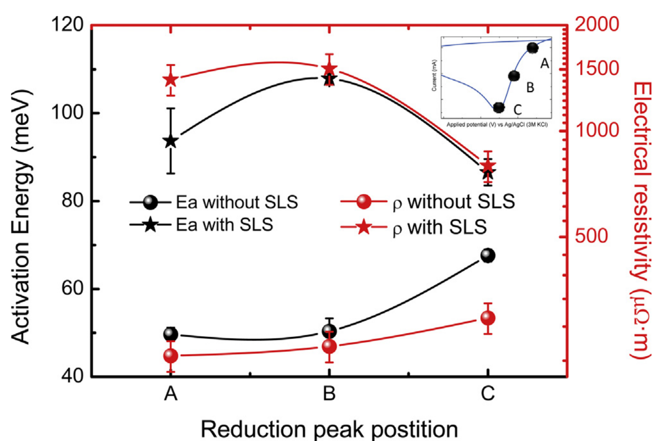

Fig. 8. Comparison of the activation energy and electrical resistivity at room temperature for the three different applied potentials for solutions without (−0.07 V, −0.10 V and −0.13 V) and with SLS (−0.18 V, −0.19 V and −0.20 V).

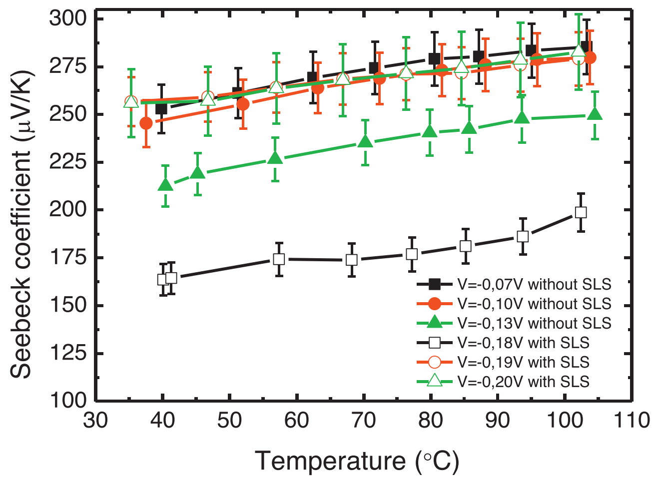

Fig. 9. Seebeck coefficient of the films grown at different applied potentials for both solutions, with (open symbols) and without (solid symbols) SLS.

coefficient slightly increases with temperature for all the films, which could be indicative of an extrinsic behavior since there should be a temperature at which the semiconductor becomes intrinsic and the Seebeck coefficient starts to decrease when the temperature is increased [42]. The highest values reached for the film grown at −0.07 V without SLS is approximately 285 μV/K, and for films with SLS at −0.20 V is approximately 284 μV/K, both near 105 °C. These values are higher than those reported by Jiang et al. for electrodeposited tellurium on polyaniline (240 μV/K) at the same temperature [20].

Finally, the power factor, which is a combination of the both aforementioned magnitudes, increases when the applied potential is either less negative in the case of the solution without SLS or more negative in the case of solution with SLS (Fig. 10). The maximum values obtained are 415 $\mu W/m{\cdot}K^2$ (without SLS) and 110 $\mu W/m{\cdot}K^2$ (with SLS) for −0.07 V and −0.20 V at 105 °C, respectively. These power factor values are of the same order of magnitude of those of bismuth telluride grown by electrodeposition [29] [35]. Moreover, the power factor values obtained near room temperature in this work, 280 $\mu W/m{\cdot}K^2$ (without SLS) and 82 $\mu W/m{\cdot}K^2$ (with SLS), are similar to those obtained by Bodiul et al., who achieved a power factor of 100 $\mu W/m{\cdot}K^2$ at room temperature for tellurium films grown by a vacuum condensation method [7]. It is noteworthy that in the case of the film prepared without SLS, an improvement by a factor of more than two has been achieved at room temperature.

Table 1
Power factor in the in plane direction, thermal conductivity in the out of plane direction, the estimated figure of merit and the assessed crystallite size calculated from the XRD analysis of the films grown with and without SLS using Scherrer formula. Figure of merit is calculated since the films are polycrystalline and not highly oriented. All the values are at room temperature.

Surfactant	Applied voltage (V)	Crystallite size (nm)	PF ($\mu W/m{\cdot}K^2$)	k (W/m·K)	zT
No	−0.07	43 ± 4	280 ± 48	1.0 ± 0.1	0.09 ± 0.01
No	−0.10	52 ± 5	246 ± 42	1.1 ± 0.1	0.07 ± 0.01
No	−0.13	60 ± 6	152 ± 26	1.3 ± 0.1	0.035 ± 0.007
SLS	−0.18	28 ± 3	19 ± 3	0.9 ± 0.1	0.006 ± 0.001
SLS	−0.19	25 ± 3	44 ± 7	0.9 ± 0.1	0.015 ± 0.003
SLS	−0.20	27 ± 3	82 ± 14	0.8 ± 0.1	0.031 ± 0.006

The thermal conductivities of the samples were also measured in order to find the growth conditions that provide the best figure of merit. As it can be seen in Table 1, the thermal conductivity values of the tellurium samples are in all the cases approximately a third of the bulk value depending on the crystal orientation (3 W/m·K)[12], which makes this material interesting from a thermoelectric point of view. The thermal conductivity values of the films that present the highest power factors are 0.8 W/m·K at V = −0.20 V (with SLS) and 1.0 W/m·K at V = −0.07 V (without SLS). It has been shown that the grain size of the tellurium films electrodeposited with the aid of the SLS is smaller than of in the case without SLS so that it could affect the phonon transport along the structure. As the grain size is reduced, phonon boundary scattering could be dominant and hence, a reduction in the thermal conductivity would be achieved [43]. In Fig. 11, the trend of the thermal conductivity as a function of the applied potential is shown. In the case of the films without SLS, the thermal conductivity decreases as the applied potential is less negative because the grain size is reduced, see Table 1, where the estimated crystallite sizes were calculated using the Scherrer equation. However, in the case of the solution with SLS, the thermal conductivity as a function of the applied potential is not as influenced. This is in agreement with the fact that all the films present approximately the same crystallite size.

The thermal conductivity values of these tellurium films is similar to the previous bismuth telluride alloys values obtained by electrodeposition, approximately 1 W/m·K [44]. From the XRD data (see Fig. 4), a polycrystalline structure can be observed so that the figure of merit can be estimated. From Table 1, the highest

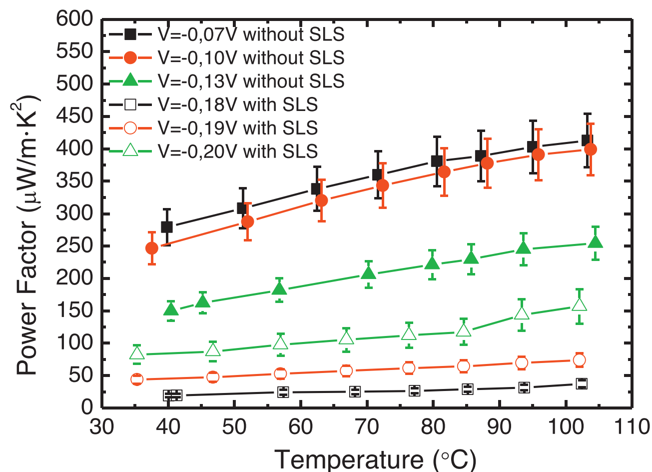

Fig. 10. Power factor of the films grown at different applied potentials for both solutions, with (open symbols) and without (solid symbols) SLS.

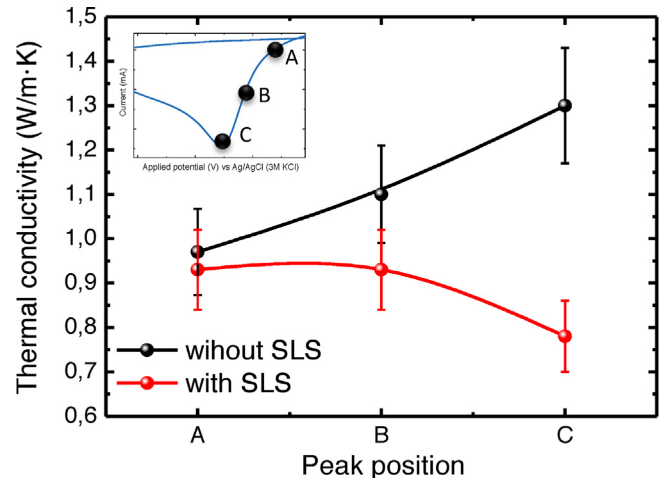

Fig. 11. Thermal conductivity as a function of the applied potential (peak position) for both solutions, with and without surfactant.

figure of merit at room temperature, 0.09, is obtained when the solution without SLS at −0.07 V is used due to its high power factor. In the case of the solution with SLS, the maximum figure of merit is 0.03 at −0.20 V because its electrical resistivity is higher due to the smaller grain size. These values are one order of magnitude higher in the estimated bulk value at room temperature, 0.008, mainly due to the great reduction in the thermal conductivity obtained by electrochemical deposition.

4. SUMMARY

A considerable change in the structure and morphology of the films appears when the surfactant sodium lignosulfonate (SLS) is added to the solution. This change implies a strong reduction in the grain size, which directly affects their thermoelectric properties. The electrical resistivity is reduced in comparison to the bulk value due to the presence of impurities. Films grown without SLS have the lowest electrical resistivity due to their lower activation energy given by their shallower impurity levels. Moreover, in the case of the SLS solution, the electrical resistivity of the films is much higher due to the reduction of the grain size of the films. The Seebeck coefficient, which shows p-type semiconductor conduction behavior, is not greatly influenced by SLS addition, with a value of approximately 285 μV/K. The power factors in the in-plane direction were 280 $\mu W/m \cdot K^2$ (without SLS) and 82 $\mu W/m \cdot K^2$ (with SLS) at room temperature and maximum values of 415 $\mu W/m \cdot K^2$ (without SLS) and 110 $\mu W/m \cdot K^2$ (with SLS) at 105 °C. This value is of the same order of magnitude than the bismuth telluride films grown by electrodeposition. Finally, the cross-plane thermal conductivity was also measured with the aid of the Photoacoustic technique and values around 1 W/m·K were obtained, which are a third of the bulk value. Finally, the figure of merit was calculated by assuming an isotropic character due to the polycrystalline properties given by the XRD data. The maximum estimated figure of merit of tellurium films is 0.09 at −0.07 V without SLS and 0.03 at −0.20 V with SLS, which are one order of magnitude higher than the bulk value.

CONFLICT OF INTEREST

The authors declare no competing financial interest

ACKNOWLEDGMENTS

The authors would like to acknowledge the financial support from ERC StG NanoTEC240497 and national project PHOMENTA MAT2011-27911.

References

[1] A.S. Epstein, H. Fritzsche, K. Lark-Horovitz, Electrical Properties of Tellurium at the Melting Point and in the Liquid State, Physical Review 107 (1957) 412–419.
[2] D. Tsiulyanu, O. Mocreac, Concentration induced damping of gas sensitivity in ultrathin tellurium films, Sensors and Actuators B: Chemical 177 (2013) 1128–1133.
[3] D. Royer, E. Dieulesaint, Elastic and piezoelectric constants of trigonal selenium and tellurium crystals, Journal of Applied Physics 50 (1979) 4042–4045.
[4] H.H. Li, P. Zhang, C.L. Liang, J. Yang, M. Zhou, X.H. Lu, G.A. Hope, Facile electrochemical synthesis of tellurium nanorods and their photoconductive properties, Crystal Research and Technology 47 (2012) 1069–1074.
[5] T. Pan, F. Zhuang, Z.-Y. Li, Absolute photonic band gaps in a two-dimensional photonic crystal with hollow anisotropic rods, Solid State Communications 129 (2004) 501–506.
[6] W. Görtz, E. Gerstenhauer, P. Grosse, Photoconducting tellurium for submillimeterwave detectors, Appl Phys A 27 (1982) 35–38.
[7] P. Bodiul, N. Bondarchuk, T. Huber, L. Konopko, A. Nikolaeva, O. Botnari, Thermoelectric Properties of Films and Monocrystalline Whiskers of Tellurium, Thermoelectrics, 2006. ICT '06. 25th International Conference on, Vienna, 2006, pp. 607–610.
[8] D.M. Rowe, CRC Thermoelectrics Handbook: Macro to Nano, in: D.M. Rowe (Ed.), CRC Press, Boca Raton, 2005.
[9] G. Fischer, G.K. White, S.B. Woods, Thermal and Electrical Resistivity of Tellurium at Low Temperatures, Physical Review 106 (1957) 480–483.
[10] V.E. Bottom, The Hall Effect and Electrical Resistivity of Tellurium, Science 115 (1952) 570–571.
[11] J.C. Perron, Thermal conductivity of Selenium-Tellurium liquid alloys, Physics Letters A 32 (1970) 169–170.
[12] R.W.P.C.Y. Ho, P.E. Liley, Thermal Conductivity of the Elements: A Comprehensive Review, Journal of Physical and Chemical reference data 3 (1974) .
[13] M.J. Capers, M. White, Structure, growth and orientation of vacuum deposited tellurium films, Thin Solid Films 8 (1971) 317–331.
[14] M.A. Dinno, M. Schwartz, B. Giammara, Structural dependence of electrical conductivity of thin tellurium films, Journal of Applied Physics 45 (1974) 3328–3331.
[15] K. Okuyama, Mobility studies of evaporated tellurium films, Thin Solid Films 33 (1976) 165–171.
[16] M.J. Capers, M. White, The electrical properties of vacuum deposited tellurium films, Thin Solid Films 15 (1973) 5–14.
[17] A.M. Phahle, Electrical properties of thermally evaporated tellurium films, Thin Solid Films 41 (1977) 235–241.
[18] A. Goswami, S.M. Ojha, Semiconducting properties of tellurium films, Thin Solid Films 16 (1973) 187–197.
[19] V. Damodara Das, N. Jayaprakash, N. Soundararajan, Thermoelectric power of tellurium thin films and its thickness and temperature dependence, J Mater Sci 16 (1981) 3331–3334.
[20] C.H. Jiang, W. Wei, Z.M. Yang, C. Tian, J.S. Zhang, Electrodeposition of tellurium film on polyaniline-coated macroporous phenolic foam and its thermopower, J Porous Mater 19 (2012) 819–823.
[21] M. Martín-González, A.L. Prieto, R. Gronsky, T. Sands, A.M. Stacy, High-Density 40nm Diameter Sb-Rich Bi2–xSbxTe3 Nanowire Arrays, Advanced Materials 15 (2003) 1003–1006.
[22] S. Bäßler, T. Böhnert, J. Gooth, C. Schumacher, E. Pippel, K. Nielsch, Thermoelectric power factor of ternary single-crystalline Sb 2Te3- and Bi2Te3-based nanowires, Nanotechnology 24 (2013) .
[23] M. Martín-González, G.J. Snyder, A.L. Prieto, R. Gronsky, T. Sands, A.M. Stacy, Direct Electrodeposition of Highly Dense 50nm Bi2Te3-ySey Nanowire Arrays, Nano Letters 3 (2003) 973–977.
[24] N. Peranio, E. Leister, W. Töllner, O. Eibl, K. Nielsch, Stoichiometry controlled, single-crystalline Bi 2Te 3 nanowires for transport in the basal plane, Advanced Functional Materials 22 (2012) 151–156.
[25] C. Frantz, N. Stein, Y. Zhang, E. Bouzy, O. Picht, M.E. Toimil-Molares, C. Boulanger, Electrodeposition of bismuth telluride nanowires with controlled composition in polycarbonate membranes, Electrochimica Acta 69 (2012) 30–37.
[26] J.-M. Song, Y.-Z. Lin, Y.-J. Zhan, Y.-C. Tian, G. Liu, S.-H. Yu, Superlong High-Quality Tellurium Nanotubes: Synthesis, Characterization, and Optical Property, Crystal Growth & Design 8 (2008) 1902–1908.
[27] M. Mo, J. Zeng, X. Liu, W. Yu, S. Zhang, Y. Qian, Controlled Hydrothermal Synthesis of Thin Single-Crystal Tellurium Nanobelts and Nanotubes, Advanced Materials 14 (2002) 1658–1662.
[28] J.-W. Liu, F. Chen, M. Zhang, H. Qi, C.-L. Zhang, S.-H. Yu, Rapid Microwave-Assisted Synthesis of Uniform Ultralong Te Nanowires, Optical Property, and Chemical Stability, Langmuir 26 (2010) 11372–11377.
[29] O. Caballero-Calero, P. Díaz-Chao, B. Abad, C.V. Manzano, M.D. Ynsa, J.J. Romero, M.M. Rojo, M.S. Martín-González, Improvement of Bismuth Telluride electrodeposited films by the addition of Sodium Lignosulfonate, Electrochimica Acta 123 (2014) 117–126.
[30] J.J. Wu, H.C. Wu, C.Z. Zhao, CdTe Solar Cells on Flexible Metallic Substrates, Advanced Materials Research 535 (2012) 2075–2078.
[31] F. Fauzi, D.G. Diso, O.K. Echendu, V. Patel, Y. Purandare, R. Burton, I.M. Dharmadasa, Development of ZnTe layers using an electrochemical technique for applications in thin-film solar cells, Semiconductor Science and Technology 28 (2013) 045005.
[32] Y.A. Ivanova, D.K. Ivanou, E.A. Streltsov, Electrochemical deposition of PbTe onto n-Si(100) wafers, Electrochemistry Communications 9 (2007) 599–604.
[33] J.P. Heremans, C.M. Thrush, D.T. Morelli, Thermopower enhancement in PbTe with Pb precipitates, Journal of Applied Physics 98 (2005) 063703–063706.
[34] M.S. Martı'n-González, A.L. Prieto, R. Gronsky, T. Sands, A.M. Stacy, Insights into the Electrodeposition of Bi2Te3, Journal of The Electrochemical Society 149 (2002) C546–C554.
[35] C. Manzano, A. Rojas, M. Decepida, B. Abad, Y. Feliz, O. Caballero-Calero, D.-A. Borca-Tasciuc, M. Martin-Gonzalez, Thermoelectric properties of Bi2Te3 films by constant and pulsed electrodeposition, Journal of Solid State Electrochemistry 17 (2013) 2071–2078.
[36] M. Martín-González, O. Caballero-Calero, P. Díaz-Chao, Nanoengineering thermoelectrics for 21st century: Energy harvesting and other trends in the field, Renewable and Sustainable Energy Reviews 24 (2013) 288–305.
[37] K.K. Mishra, K. Rajeshwar, A re-examination of the mechanisms of electrodeposition of CdX and ZnX (X = Se, Te) semiconductors by the cyclic photovoltammetric technique, Journal of Electroanalytical Chemistry 273 (1989) 169–182.

[38] F. Xiao, B. Yoo, M.A. Ryan, K.H. Lee, N.V. Myung, Electrodeposition of PbTe thin films from acidic nitrate baths, Electrochimica Acta 52 (2006) 1101–1107.
[39] H. Hu, X. Wang, X. Xu, Generalized theory of the photoacoustic effect in a multilayer material, Journal of Applied Physics 86 (1999) 3953–3958.
[40] G. She, W. Shi, X. Zhang, T. Wong, Y. Cai, N. Wang, Template-Free Electrodeposition of One-Dimensional Nanostructures of Tellurium, Crystal Growth & Design 9 (2008) 663–666.
[41] J. Szymczak, S. Legeai, S. Diliberto, S. Migot, N. Stein, C. Boulanger, G. Chatel, M. Draye, Template-free electrodeposition of tellurium nanostructures in a room-temperature ionic liquid, Electrochemistry Communications 24 (2012) 57–60.
[42] P. Pichanusakorn, P. Bandaru, Nanostructured thermoelectrics, Materials Science and Engineering: R: Reports 67 (2010) 19–63.
[43] M. Takashiri, K. Miyazaki, S. Tanaka, J. Kurosaki, D. Nagai, H. Tsukamoto, Effect of grain size on thermoelectric properties of n-type nanocrystalline bismuth-telluride based thin films, Journal of Applied Physics 104 (2008) 084302.
[44] C. Schumacher, K.G. Reinsberg, R. Rostek, L. Akinsinde, S. Baessler, S. Zastrow, G. Rampelberg, P. Woias, C. Detavernier, J.A.C. Broekaert, J. Bachmann, K. Nielsch, Optimizations of Pulsed Plated p and n-type Bi2Te3-Based Ternary Compounds by Annealing in Different Ambient Atmospheres, Advanced Energy Materials 3 (2013) 95–104.